arXiv:2607.16873v1 [cs.CV] 18 Jul 2026

InfoDense: Density-Aware Regional Decisive Replay for Memory-Efficient Incremental Face Forgery Detection

Jikang Cheng[2*], Hao Shen[1*], Xueyi Zhang[3], Guangcheng Wang[4]
Zhongyuan Wang[5], Renye Yan[2†], Baojin Huang[1†]

[1]Huazhong Agricultural University, [2]Peking University
[3]National University of Singapore, [4]Nantong University
[5]Wuhan University

[*]These authors contributed equally to this work
[†]Correspondence to: victory@stu.pku.edu.cn, huangbaojin@mail.hzau.edu.cn

Abstract

The rapid evolution of face forgery techniques has introduced an increasing variety of manipulations. Incremental Face Forgery Detection (IFFD), which incrementally adds new forgery data to fine-tune previously trained models, has emerged as a promising approach to handle evolving forgery threats. However, conventional replay-based IFFD methods suffer from catastrophic forgetting. Storing full historical images under limited memory often either fails to preserve subtle forgery cues or introduces domain bias, reducing the model's ability to learn intrinsic and transferable manipulation characteristics. In this paper, we propose a Density-Aware Regional Decisive replay strategy, termed **InfoDense**, to address these challenges. InfoDense prioritizes artifact-dense and forgery-critical regions, significantly reducing storage requirements while maintaining high-fidelity forgery evidence. We first introduce **InfoDense Cut** to localize decisive patches using CLIP-based embeddings. Then, **InfoDense Select** ranks candidate segments by combining latent-space representativeness and decisive patch counts, ensuring both diversity and information density in the replay buffer. Finally, **InfoDense Fuse** reconstructs unbiased training inputs by adaptively merging stored segments with current-task samples, enhancing knowledge retention and generalization. Extensive experiments on challenging incremental deepfake benchmarks demonstrate that InfoDense effectively mitigates catastrophic forgetting while improving cross-domain generalization.

1 Introduction

The rapid advancement of generative technologies has led to increasingly diverse and realistic forgery faces, posing serious threats to multimedia security and social trust. One line of research seeks to address this challenge by training forgery detection models with strong generalization ability under limited data conditions, so as to improve robustness to unseen forgeries. However, generalization-oriented approaches (Sun et al. 2022; Cao et al. 2022; Huang et al. 2023; Yan et al. 2024a; Cheng et al. 2024, 2025b) can only partially handle unknown forgery patterns and still struggle to cope with the continuous evolution of forgery techniques. To this end, Incremental Face Forgery Detection (IFFD) has recently attracted growing attention, aiming to progressively learn new forgery types while maintaining reliable detection performance on previously learned ones.

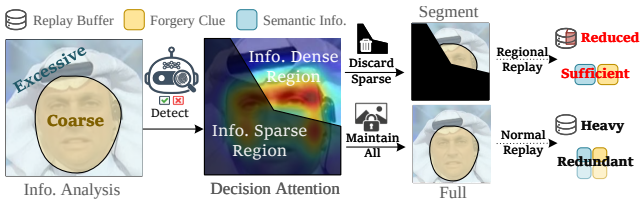

Figure 1: Intuitive impression of our motivation: replaying InfoDense segment instead of replaying redundant full faces.

IFFD methods typically mitigate catastrophic forgetting by replaying representative samples during the learning of new data. Common strategies include central sample replay (Pan et al. 2023), hard sample replay (Pan et al. 2023), adversarial perturbation–based replay (Sun et al. 2025), mixed prototypes (Tian et al. 2024), and sparse uniform replay (Cheng et al. 2025a). However, these replay-based approaches inevitably require storing raw historical samples, resulting in non-negligible memory overhead and potential privacy risks. Please refer to Appendix Section 1 for detailed illustrations of ***Related Work***. Notably, face images exhibit strong structural regularities, such as bilateral symmetry and the spatial concentration of discriminative cues. For deepfake detection, the information required for effective replay mainly concerns identity-related features, forgery artifacts, and domain-specific patterns. These cues are typically localized and redundantly distributed across symmetric facial regions rather than uniformly over the entire face. Hence, storing the full face image may be unnecessary to preserve replay knowledge, while selectively retaining informative regions can sufficiently maintain the critical information needed to mitigate forgetting in IFFD.

Motivated by the above observations, we aim to design a **regional decisive replay** strategy that preserves essential forgery knowledge while significantly reducing storage cost. As shown in Fig. 1, we model and visualize the decisive attention of samples during detector training. According to the resulting attention distribution, forgery face images

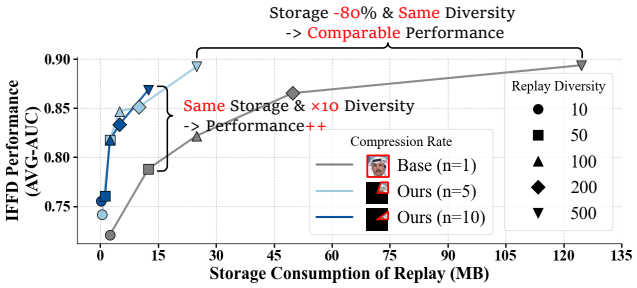

Figure 2: Performance impression on compressing redundant facial information. The results are obtained with Protocol 1 (see Sec. 3.1). **n** in Compression Rate denotes $\frac{1}{n}$ segment of one intact image is used for replay. Replay Diversity is represented by the number of image samples stored in the replay set. With significantly reduced storage, two different versions of our approach achieve comparable performance against the baseline, indicating the redundancy of using intact face images as the replay samples.

can be conceptually divided into **information-dense** and **information-sparse** regions. The **former** is sufficient to capture critical domain characteristics and **forgery traces**, while the **latter** mainly contains **redundant content**. Furthermore, the empirical results in Fig. 2 validate the substantial potential of compressing redundant facial information. Even when only a fraction of each image is retained, the detection performance remains highly competitive, indicating that intact facial images contain considerable redundancy for replay. Based on this insight, we preferentially retain information-dense regions during replay, **enabling effective knowledge preservation with significantly reduced memory cost**. As a result, more historical samples can be stored under the same budget, alleviating catastrophic forgetting. Meanwhile, concentrating replay on compact yet decisive regions encourages the detector to focus on intrinsic forgery cues, thereby improving generalization to unseen manipulations.

In this paper, we propose a Density-Aware Regional Decisive replay strategy, termed InfoDense, for memory-efficient incremental deepfake detection. The goal is to preserve forgery-critical information under limited replay capacity. We first introduce **InfoDense Cut** to estimate the regional density of decisive forgery cues. Patch-level image tokens are extracted using a CLIP-based encoder. Each token is assigned a forgery-decisive score based on its similarity to forgery-representative text embeddings. The top-K patches are selected as Decisive Patches to localize the most discriminative regions. We then perform **InfoDense Select** to rank candidate segments. The ranking is based on a weighted combination of latent-space centroid distance and decisive patch count. The top-m segments are stored in the replay buffer to ensure both representativeness and information density. Finally, we apply **InfoDense Fuse** to adaptively combine stored segments with current-task samples. This process reconstructs complete training inputs and enables effective and unbiased replay. It also enriches fine-grained forgery evidence and mitigates catastrophic forgetting during incremental learning. Our contributions can be summarized as follows: (1) By exploiting the inherent redundancy in facial information, InfoDense significantly reduces storage requirements. Under the same memory budget, it enables a multiplicative increase in replay diversity, thereby effectively alleviating catastrophic forgetting. (2) InfoDense distills core forgery-decisive cues and reuses them across multiple tasks, encouraging the model to capture intrinsic forgery characteristics rather than task-specific artifacts, thus improving generalization ability. (3) Since the replay buffer stores only compact decisive regions instead of complete facial images, InfoDense naturally mitigates potential privacy risks associated with data replay, making it more suitable for practical deployment.

2 Proposed Method

To compress the redundant information in the facial data, thus improving the diversity and information density under the limit of the same storage consumption, we propose a unified framework termed InfoDense that can cut, select, and utilize the regional segments with dense information for replay. The overall pipeline can be found in Fig. 3.

2.1 Rationale Behind Compressing Facial Information

Facial images contain substantial structural redundancy due to the strong spatial regularity and identity consistency of human faces. A large portion of a face, including smooth skin regions such as the cheeks, forehead, and jaw area, exhibits a homogeneous appearance that remains stable across frames, poses, and expressions. These regions primarily encode identity-related information and contribute little to forgery detection. In contrast, deepfake detectors mainly rely on subtle local inconsistencies introduced during synthesis and blending, which are typically concentrated around semantically sensitive regions such as the eyes, mouth, nose boundary, and facial contour. As a result, the majority of facial pixels provide highly correlated and repetitive signals from the perspective of the detection objective.

Moreover, recent deepfake generation methods aim to preserve global facial structure and identity while minimizing perceptual artifacts, which further increases redundancy in non-critical regions. The discriminative evidence is therefore sparse relative to the full image, and storing entire facial images for replay retains large amounts of non-informative content. By compressing facial information and preserving only forgery-decisive regions, the replay strategy focuses on task-relevant evidence while discarding redundant identity-consistent signals. This selective retention reduces memory consumption and enables more diverse replay samples under a fixed storage budget, which is particularly beneficial for incremental deepfake detection.

2.2 Replay Selection

Regional Density of Decisive Information. First, we manage to expose the region in a single face that is the most decisive for the judgment of the detectors. At present, a variety of well-established techniques have been developed to

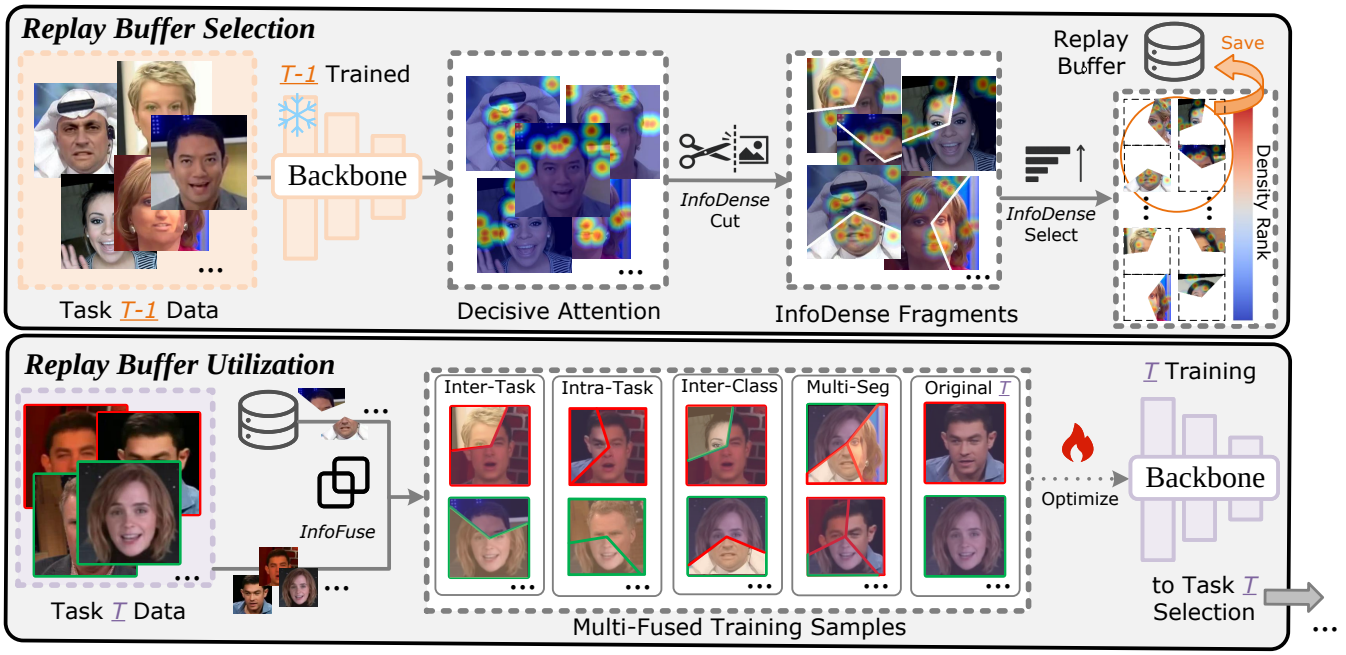

Figure 3: The overall pipeline of the proposed InfoDense. We extract informative regional segments via a cut-and-select strategy. These segments are then used in replay learning to mitigate catastrophic forgetting and enhance generalization.

obtain the decision-related attention regions of a model (either CNN-based (Selvaraju et al. 2017; Chattopadhay et al. 2018) or ViT-based (Bousselham et al. 2025; Chefer, Gur, and Wolf 2021)) with respect to a given input image. Building upon these approaches, we incorporate forged information and propose to leverage the text-image alignment capacity of CLIP to highlight the forgery-related similarity of different patches. Specifically, given an input image $\mathbf{x}^{t-1} \in \mathbb{I}^{t-1}$, where $\mathbb{I}^{t-1}$ denotes the $t-1$ task, we can have a CLIP-based detector $f(\cdot, \theta^{t-1})$ with $t-1$ trained parameters θ^{t-1}. We can then obtain a series of image tokens using $t-1$ encoder ($E(\cdot)$) as $E(\mathbf{x}^{t-1}) = \{\mathbf{z}_{cls}, \mathbf{z}_{(1,1)}, ..., \mathbf{z}_{(n,n)}\}$. Subsequently, to evaluate the forgery-decisive score (δ) of each token, we compare the similarity of each token with the forgery-representative token ($\mathbf{z}_f$), which is obtained by encoding forgery-representative prompts via the text encoder. Since both text and image tokens are pre-trained to be mapped to the consistent latent space, they can be directly leveraged to compare similarity. Formally, the forgery decisive score δ of the patch at location (i, j) is computed as:

$$\delta_{(i,j)} = \text{Sim}(\mathbf{z}_{(i,j)}, \mathbf{z}_f), \tag{1}$$

where $\text{Sim}(\cdot)$ calculates the cosine similarity. Appendix 7.2 provides an extensive analysis and empirical support for adopting this CLIP-based attention algorithm, a robust approach widely validated in prior work (Cui et al. 2025a; Zhou et al. 2026). Finally, we sort the patches by their δ scores and retain the top 10 as the Decisive Patches ($\mathbf{P}_\text{D} = \{\mathbf{p}_1, ..., \mathbf{p}_{10}\}$) for each image.

InfoDense Cut. Here, we need to utilize the decisive patches $\mathbf{P}_\text{D}$ to guide the cutting extraction of the most info-dense partial region in each image. To achieve this, we first consider deploying ClockMix (Cheng et al. 2025b) as the cutting manner to extract regions that are dense in forgery information while maintaining semantic uniformity. Since ClockMix has already been proven to cut out segments in face forgery that evenly include identity, forgery, and background, we only need to focus on how to compute the ClockMix-segment that contains the maximum number of decisive patches in each image. Specifically, we employ a two-pointer scanning strategy. Given an angle ratio ofthe extracted region (n) and two rays (v_1) and (v_2) with an angle of $\frac{360}{n}$, these two rays will scan all angles starting from the origin vertical one, ultimately obtaining the regional segment ($\mathbf{s}$) that contains the largest count of decisive patches as:

$$\mathbf{s} = \text{Cut}(\mathbf{x}) = \underset{\alpha \in [0,\, 360-360/n)}{\arg\max} \left(\text{Count}_\text{D}(\text{Seg}(v_1, v_2, \alpha))\right), \tag{2}$$

where $\text{Count}_\text{D}(\text{Seg}) = \sum_{\mathbf{p} \in \mathbf{P}_\text{D}} \mathbf{I}\left(\mathbf{p} \text{ within } \text{Seg}\right)$ represents the decisive patch count within the segment, $\mathbf{I}(\cdot)$ is an indicator that returns 1 when the input expression is true, α is the angle from begin to v_1. Based on the aforementioned algorithm, we can obtain the InfoDense Cut Segment set $\mathbf{S} = \{\mathbf{s}, ...\}$ corresponding to each image $\{\mathbf{x}, ...\} \in \mathbb{I}^{t-1}$.

InfoDense Select. Given a set of InfoDense Cut Segments, we further need to select the most information-dense one to be stored in the final replay buffer. Here, we consider both the latent-space centroid similarity (Pan et al. 2023) and the count of included decisive patches for the replay selection. This is because the central data of the distribution contains the most representative information of the overall dataset,

while the decisive patch count represents the information that plays a critical role in forgery detection. Therefore, we combine the centroid distance and patch count with a weighted sum, which is then used for sorting.

$$\hat{\mathbf{S}} = \text{sort}\left(\mathbf{S}, \text{Score}(\mathbf{s}_i)\right), \tag{3}$$

where the selection score of each candidate segment $\mathbf{s}_i$ is defined as

$$\text{Score}(\mathbf{s}_i) = \lambda \cdot \widetilde{R}_i + (1-\lambda) \cdot \widetilde{D}_i. \tag{4}$$

Here, $R_i = \cos(\mathbf{c}, f(\mathbf{x}_i))$ measures the latent-space representativeness of the source image $\mathbf{x}_i$, and $D_i = \text{Count}_{\text{D}}(\mathbf{s}_i)$ denotes the number of decisive patches covered by the segment $\mathbf{s}_i$. The centroid feature is computed as $\mathbf{c} = \mathbb{E}_{\mathbf{x}\in\mathbb{I}^{t-1}}[f(\mathbf{x})]$, where $\mathbb{E}[\cdot]$ denotes the expectation operator. Since R_i and D_i have different numerical ranges, we normalize both terms to $[0, 1]$ over the candidate segment set before combination, yielding $\widetilde{R}_i$ and $\widetilde{D}_i$.

2.3 Replay Utilization

InfoFuse. While conventional replay data are intact and ready for direct training, InfoDense segments are inherently fragmented and incompatible with model ingestion. Therefore, we reconstruct intact samples by fusing these fragmented replays with current-task data $\mathbb{I}^t$. Essentially, current-task samples serve as the base, onto which InfoDense segments are integrated to retain previous-task knowledge. Formally, for a replay segment $\mathbf{s} \in \mathbf{S}^{t-1}$, a current-task sample $\mathbf{x} \in \mathbb{I}^t$, and its binary mask $\mathbf{M_s}$, the fusion is formulated as:

$$\mathbf{x}^t_{\text{train}} = \text{InfoFuse}(\mathbf{x}, \mathbf{s}) = (1 - \mathbf{M_s}) \odot \mathbf{x} + \mathbf{M_s} \odot \mathbf{s}, \tag{5}$$

where $\odot$ denotes element-wise multiplication, and $\mathbf{M_s} = 1$ inside the replay region and 0 otherwise.

Multi-Fused Samples. Due to the various existence of current task data, past task data, and the combinations of their real/fake labels, the strategy behind their pairings and the labeling requires further analysis. We adopt the labeling strategy among real/fake combinations from ClockMix (Cheng et al. 2025b), where any inclusion of "fake" segment is labeled as fake. This is because we want to ensure that all real/fake data in the replay buffer is effectively utilized for real/fake judgment training. Then, the combinations among previous and current tasks are newly introduced by our mixing paradigm and need to be carefully designed here. For simplicity, we use (t-1) to represent all past task data.

1. **(t) & (t-1) inter-task**: We perform a full combination of the real/fake labels from (t-1) and (t) (i.e., $2 \times 2 = 4$ combinations). By mixing data with different labels for replay, we impose a constraint that helps the model learn the full information in the replay buffer and prevents class bias.

2. **(t) intra-task**: To ensure that the model maintains desensitization with fused images that contain junctions, we also perform random mixing of real/fake labels within the (t) task. This avoids spurious correlations where fused samples are misattributed to task (t-1), thereby preventing task bias in the model's learning process.

3. **Multi-Seg**: Following Eq. 5, past segments from task (t-1) are integrated with various current-task instances (t). This fusion maximizes the retention of historical knowledge and reinforces the supervisory signal of past data to prevent forgetting. Additionally, such multi-segment fusion boosts sample diversity and captures finer-grained subtle forgery artifacts.

All of the aforementioned types of fused samples, along with the original images from the (t)-task, form a mini-batch for training the (t)-task model ($f(\cdot, \theta^t)$). In summary, Multi-Fused samples have the following three advantages: 1. They allow fragmented regional replay data to be effectively utilized in an intact form for replay training. 2. The fusion strategy prevents class and task biases that could arise from the introduction of fusion among different tasks and labels. 3. Fused samples contain more diverse and fine-grained information, enhancing the model's ability to learn generalizable and subtle knowledge.

3 Experimental Results

3.1 Experimental Settings

Datasets. To construct a comprehensive benchmark that covers diverse domains and forgery techniques, we utilize a wide range of datasets. For classical benchmarks, we adopt FaceForensics++ (FF++) (Rossler et al. 2019), DeepFake Detection Challenge Preview (DFDCP) (Dolhansky et al. 2020), Celeb-DF-v2 (CDF) (Li et al. 2020b), DeepFake Detection (DFD) (Nick Dufour and Andrew Gully 2019), WildDeepfake (WDF) (Zi et al. 2020), and UADFV (Li, Chang, and Lyu 2018). To account for emerging generative threats, we further incorporate DiT and SDv21 from DF40 (Yan et al. 2024b), and SDv21 from DiffusionFace (Chen et al. 2024). Although two datasets share the name SDv21, they originate from different sources. In our IFFD protocol, we use the SDv21 version from DiffusionFace (Chen et al. 2024) for training and evaluation, while the SDv21 version from DF40 (Yan et al. 2024b) is reserved as a hold-out set to assess generalization ability.

Incremental Protocols. We design two complementary incremental evaluation protocols to systematically assess the model's plasticity and stability under evolving forgeries:

- **Protocol 1: Training:** The model is incrementally trained on the sequence {FF++, DFDCP, CDF, SDv21 (DiffusionFace)}. **Testing:** After completing training on SDv21 (DiffusionFace), the resulting model is regarded as the final model. Forgetting is evaluated by testing this final model on the previously seen datasets (FF++, DFDCP, and CDF). *Generalization* is assessed by evaluating its performance on SDv21 (DF40) as a held-out diffusion benchmark, as well as additional unseen datasets including UADFV, WDF, and DFD.
- **Protocol 2:** Sequence of {DFDCP, SDv21 (DiffFace), DiT, CDF} is introduced to simulate diverse domain shifts and heterogeneous generation architectures, e.g., Diffusion Transformers (DiT), thereby imposing a rigorous evaluation of the detector's robustness and adaptability.

Table 1: Performance comparison for face forgery detection based on Protocol 1. The two "Avg." values denote the average detection AUC over the incremental datasets and the cross-dataset evaluation sets, respectively. The best are denoted in bold.

Method	Venue	Incremental Dataset					Cross-dataset				
		FF++	DFDCP	CDF	PD ↓	Avg.	SDv21	UADFV	WDF	DFD	Avg.
L-Bound	–	64.51	61.10	83.42	11.91	69.67	43.36	88.31	51.90	63.87	61.86
LwF (Li and Hoiem 2017)	TPAMI' 17	65.32	71.48	76.91	10.86	71.24	50.12	87.45	74.38	69.24	70.30
iCaRL (Rebuffi et al. 2017)	CVPR' 17	62.75	74.36	85.92	10.91	74.34	58.47	86.02	60.73	74.88	70.03
DER (Yan, Xie, and He 2021)	CVPR' 21	64.03	79.77	94.68	7.35	79.49	66.91	85.10	65.89	80.56	74.62
CoReD (Kim, Tariq, and Woo 2021)	MM' 21	66.84	82.15	91.37	6.92	80.12	72.84	84.92	68.77	85.34	77.97
DFIL (Pan et al. 2023)	MM' 23	77.66	86.48	95.45	6.48	86.53	76.53	84.87	70.01	87.03	79.61
HDP (Sun et al. 2025)	IJCV' 24	73.34	81.96	92.90	6.59	82.73	60.08	80.82	72.59	80.01	73.38
SUR-LID (Cheng et al. 2025a)	CVPR' 25	83.21	80.81	94.85	6.87	86.29	72.02	93.43	66.50	67.50	74.86
GPL (Zhang et al. 2025)	ICCV'25	77.92	85.43	91.99	5.91	85.11	83.05	**95.17**	72.12	80.09	82.61
Ours	–	**84.11**	**89.41**	**97.75**	**4.52**	**90.42**	**97.88**	94.71	**79.38**	**88.13**	**90.03**

Table 2: Ablation study on compression strategies. **nSeg** denotes the average number of decisive patches per replay segment.

Method	nSeg	Incremental Dataset					Cross-dataset				
		FF++	DFDCP	CDF	PD ↓	Avg.	SDv21	UADFV	WDF	DFD	Avg.
Base(DFIL)	–	77.66	86.48	95.45	6.48	86.53	43.36	88.31	51.90	63.87	61.86
JPEG (Q=50)	–	73.22	89.11	94.34	4.84	85.55	71.99	88.24	70.54	82.73	78.37
JPEG (Q=95)	–	79.26	84.03	91.45	5.16	84.91	79.29	94.22	79.28	91.40	86.04
CIM(Luo et al. 2023)	–	83.12	87.18	94.94	4.97	88.41	89.04	94.60	71.82	82.20	84.41
CutMix	3.86	72.34	76.24	90.38	6.72	79.65	57.14	93.52	75.21	73.98	74.96
CutMix+$\mathbf{P}_{\mathrm{D}}$	7.52	79.83	83.13	93.94	6.31	85.63	62.70	87.29	68.31	84.46	75.69
ClockMix	3.34	78.12	87.00	93.85	6.01	86.32	83.40	84.56	73.78	81.20	80.58
InfoDense (Ours)	8.31	84.11	89.41	97.75	4.52	90.42	97.88	94.71	79.38	88.13	90.03

Implementation Details. Our method is implemented in PyTorch with the pre-trained CLIP ViT-L/14 as the backbone network. All input images are resized to 224×224 to satisfy the encoder requirements. The model is optimized using the Adam optimizer with an initial learning rate of 2×10^{-4}, a batch size of 8, and is trained for 5 epochs per task. All experiments are conducted on a single NVIDIA Tesla A100 GPU. For evaluation, frame-level Area Under the Curve (AUC) is deployed as the primary metric to measure detection performance. To further quantify catastrophic forgetting, we introduce a Performance Dropping rate (PD), defined as $PD = M_0 - M_N$, where M_0 represents the average AUC in the base session and M_N represents the average AUC in the final session.

3.2 Comparison with IFFD Baselines

We evaluate InfoDense against state-of-the-art incremental face forgery detection methods under Protocol 1 to assess continual learning stability and cross-domain generalization. As shown in Tab. 1, InfoDense achieves the lowest PD, indicating strong resistance to catastrophic forgetting on previously learned datasets, including FF++, DFDCP, and Celeb-DF. Unlike methods that replay complete historical images with limited diversity, InfoDense removes task-irrelevant background regions, enabling more diverse replay under the same memory budget and improving stability across incremental tasks.

Additionally, InfoDense guides the model to focus on concentrated and decisive forgery fragments rather than entire facial regions, encouraging intrinsic and transferable forgery cues instead of dataset-specific biases. Consequently, it achieves clear ***cross-domain gains*** and significantly outperforms competitors such as SUR-LID on challenging unseen datasets like WDF. More detailed comparisons are provided in Appendix Tab. 8 and Fig. 11.

3.3 Ablation Study on Compression Strategies

Comparison with Global Compression Baselines. A comparison with global compression baselines, including JPEG at different compression ratios and CIM, is presented in Tab. 2. Moderate global compression enables more historical samples to be stored and brings a slight performance improvement over the uncompressed baseline. However, as the compression ratio increases, subtle high-frequency artifacts that are critical for deepfake detection are progressively destroyed, resulting in significant performance degradation. This phenomenon highlights the intrinsic limitation of global lossy compression, which reduces memory usage at the expense of indiscriminately damaging essential forgery traces. In contrast, InfoDense avoids this trade-off by adopting spatial compression rather than quality compression. Task-irrelevant background regions are removed, while the original, uncompressed pixels in information-dense areas are strictly preserved. This design maintains high-fidelity forgery cues and ensures more robust knowledge preservation under the same memory budget.

Table 3: Ablation study on regional selection strategies. **nSeg** denotes the average decisive patches per replay segment.

Method	nSeg	Incremental Dataset					Cross-dataset				
		FF++	DFDCP	CDF	PD ↓	Avg.	SDv21	UADFV	WDF	DFD	Avg.
Random	3.34	79.02	78.51	92.23	6.58	83.25	83.40	84.56	73.78	81.20	80.58
Center	6.46	80.26	84.20	94.93	5.80	86.46	84.87	89.32	72.86	76.58	80.90
Center+Hard	6.64	80.46	83.15	96.11	5.56	86.57	79.00	83.74	70.48	83.80	79.25
Ours	8.31	84.11	89.41	97.75	4.52	90.42	97.88	94.71	79.38	88.13	90.03

Table 4: Ablation study on inter-task and intra-task fusion strategies. $(t-1)\&(t-1)$ and $(t-1)\&(t)$ denote isolated historical self-fusion and inter-task fusion without intra-task mixing, respectively.

Method	Incremental Dataset					Cross-dataset				
	FF++	DFDCP	CDF	PD ↓	Avg.	SDv21	UADFV	WDF	DFD	Avg.
$(t-1)\&(t-1)$	63.75	61.27	80.11	12.23	68.37	63.29	86.65	59.88	66.63	69.11
$(t-1)\&(t)$	79.23	89.75	94.72	4.91	87.90	72.74	96.19	67.62	80.74	79.32
Ours	84.11	89.41	97.75	4.52	90.42	97.88	94.71	79.38	88.13	90.03

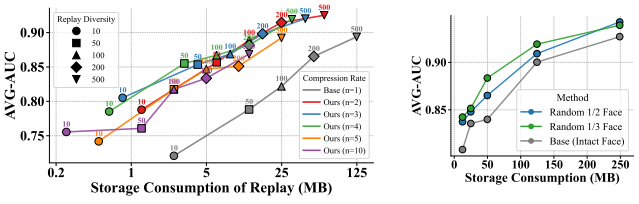

Figure 4: Storage-performance Pareto frontier under varying replay budgets. (Left) Results evaluated on Protocol 1. (Right) Results evaluated on Protocol 2.

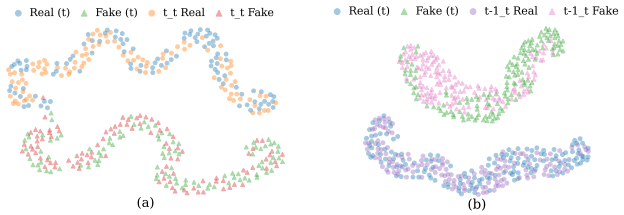

Figure 5: UMAP visualization of the latent space. (a) Original Task t samples *vs.* intra-task self-fused samples. (b) Original Task t samples *vs.* inter-task replay samples.

Impact of Regional Shapes and Patch Selection. We analyze region shapes and patch selection strategies in Tab. 2, where Cut/Clock denote rectangular/fan-shaped regions, Mix denotes random sampling, and P_D or InfoDense uses decisive patch density for selection.

1. Rectangular vs. Fan-shaped. Under random sampling, fan-shaped ClockMix consistently outperforms rectangular CutMix. This is because facial structures and forgery artifacts often follow a center-symmetric distribution, making sectors radiating from the facial center more likely to preserve key structural and manipulation cues, while random rectangles may miss the facial center.

2. Random vs. Density-Aware Patch Selection. Density-aware selection with decisive patches P_D clearly improves information concentration. Random sampling covers few decisive regions, as reflected by the low nSeg values of CutMix and ClockMix. In contrast, CutMix+P_D and InfoDense substantially increase decisive-region coverage. By combining center-symmetric fan-shaped regions with forgery-cue density, InfoDense achieves a better trade-off between spatial compression and discriminative performance.

3.4 Ablation on Selection and Fusion Strategies

Effectiveness of Selection Strategy. Tab. 3 compares InfoDense with Random, Center, and Center+Hard sampling. For Center, the decisive patch count is set to zero, and selection relies only on latent-space centroid distance to preserve distribution representativeness. Although central samples and decision-boundary hard samples slightly outperform random selection, they cannot ensure that sampled fragments contain forgery artifacts, yielding insufficient task-relevant cues. In contrast, InfoDense dynamically combines centroid distance with decisive patch count, filtering redundant backgrounds and enriching the replay buffer with artifact-rich fragments. This dual-metric strategy mitigates catastrophic forgetting and provides higher-quality replay data, leading to stronger generalization across unseen domains.

Effectiveness of Fusion Strategy. To validate InfoFuse, we compare it with two simplified variants: isolated historical self-fusion ($(t-1)\&(t-1)$) and inter-task-only fusion ($(t-1)\&(t)$). As shown in Tab. 4, isolated self-fusion causes severe catastrophic forgetting, as reconstructing replay samples only from historical data introduces a large domain gap from pristine current-task images and amplifies task bias. Inter-task-only fusion, which pastes historical segments onto current images, partially reduces this gap but

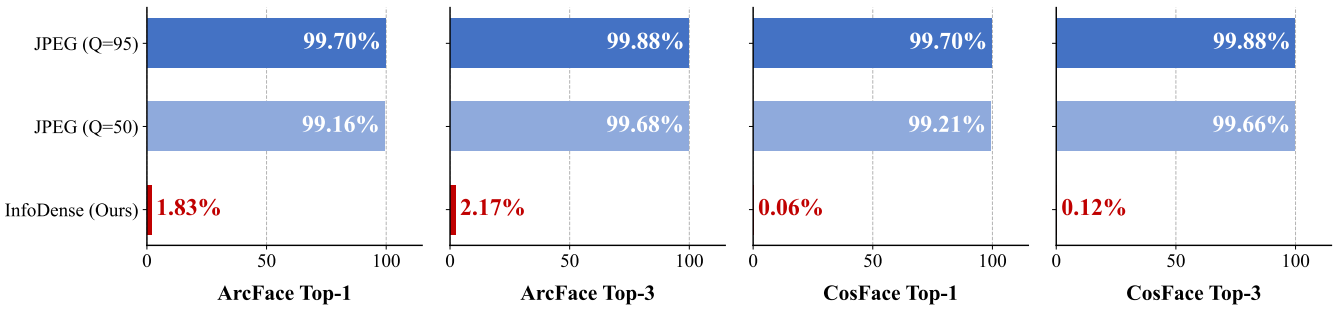

Figure 6: Quantitative analysis of identity privacy protection. Top-1 and Top-3 recall rates denote the probability of retrieving original identities from replay samples via face recognition (*e.g.*, ArcFace, CosFace). Lower rates imply less identity leakage.

remains sub-optimal. Without intra-task mixing on current data, the model may exploit artificial fusion boundaries as shortcuts for task identity instead of learning intrinsic forgery patterns. In contrast, InfoFuse jointly performs inter-task and intra-task mixing, exposing the model to fusion boundaries across data distributions. This reduces boundary sensitivity, encourages attention to genuine forgery traces, and improves both knowledge retention and generalization.

3.5 Storage Efficiency and Redundancy

Here, we extensively analyze InfoDense storage efficiency and validate the intrinsic redundancy hypothesis in IFFD from two aspects: storage-performance trade-off and empirical redundancy limits.

Performance Evaluation on Storage Efficiency. In practical deployment, maximizing detection accuracy under limited storage is a key Pareto optimization problem. We compare InfoDense with the full-image replay baseline DFIL under different compression ratios. As shown in Fig. 4, InfoDense consistently achieves a superior Pareto frontier. Under the same memory budget, storing more compressed, information-dense fragments significantly outperforms storing fewer complete images. For instance, fragments at one quarter of the original size achieve higher accuracy than storing the same number of intact images while using much less memory. These results show that density-aware selection removes redundant background content and preserves richer forgery cues under strict storage constraints.

Verification of Facial Redundancy. To empirically validate the redundancy of face forgery data, we conduct a supplementary experiment with random fan-shaped cropping on a naive CNN backbone (Fig. 4 Right). By discarding strategic selection and randomly extracting regional segments, we assess the structural resilience of forgery cues. Surprisingly, random extraction consistently outperforms full-image replay, confirming that forgery traces are highly redundant and center-symmetric. This supports our motivation that storing entire faces limits replay diversity, while even randomly sampled partial regions can retain sufficient discriminative information for robust incremental replay.

3.6 Visualization Analysis on InfoDense Fuse

To show that segment fusion preserves deepfake discriminability without seaming-induced confusion, we visualize the latent space using UMAP (McInnes, Healy, and Melville 2018). Fig. 5(a) shows original Task t samples and intra-task self-fused samples. The fused features align well with the original real and fake clusters, indicating that fusion preserves intrinsic class distributions. Fig. 5(b) compares original Task t samples with inter-task replay samples, where Task $t-1$ segments are fused onto Task t. The replay features largely overlap with the corresponding real and fake domains while maintaining clear class separability. This confirms that InfoDense Fuse constructs valid replay data that preserves core forgery cues and supports historical knowledge accumulation without distorting the feature space.

3.7 Privacy Quantitative Analysis

A key concern in replay-based incremental learning is privacy leakage from stored historical data. To evaluate privacy preservation, we measure the identity retrieval recall of stored samples against original faces using ArcFace (Deng et al. 2019) and CosFace (Wang et al. 2018). As shown in Fig. 6, global compression methods still retain near-perfect retrieval recall even under high compression, as they preserve the holistic facial topology required for identity recognition. In contrast, InfoDense disrupts this structure by retaining only localized forgery-decisive fragments, preventing the recognition of coherent identity embeddings and reducing retrieval recall to near zero. This shows that InfoDense improves storage efficiency while serving as an effective de-identification mechanism for privacy-sensitive deployment. Further Privacy analysis can be found in Appendix 7.9.

4 Conclusion

In this paper, we introduce InfoDense, a Density-Aware Regional Decisive replay strategy for memory-efficient Incremental Face Forgery Detection. By actively leveraging facial image redundancy, InfoDense extracts compact, artifact-dense regions, drastically reducing overall storage costs and boosting replay sample diversity within the same memory budget. Furthermore, extracting forgery-decisive cues across continuous tasks compels the detection network to learn

transferable manipulation characteristics rather than overfitting to task-specific artifacts. Extensive evaluations on multiple challenging incremental benchmarks fully validate the effectiveness of our InfoDense in maximizing knowledge retention and cross-domain generalizability.

References

Bousselham, W.; Boggust, A.; Chaybouti, S.; Strobelt, H.; and Kuehne, H. 2025. Legrad: An explainability method for vision transformers via feature formation sensitivity. In *Proceedings of the IEEE/CVF International Conference on Computer Vision*, 20336–20345.

Buslaev, A.; Iglovikov, V. I.; Khvedchenya, E.; Parinov, A.; Druzhinin, M.; and Kalinin, A. A. 2020. Albumentations: fast and flexible image augmentations. *Information*, 11(2): 125.

Cao, J.; Ma, C.; Yao, T.; Chen, S.; Ding, S.; and Yang, X. 2022. End-to-End Reconstruction-Classification Learning for Face Forgery Detection. In *IEEE Conference on Computer Vision and Pattern Recognition*, 4113–4122.

Chattopadhay, A.; Sarkar, A.; Howlader, P.; and Balasubramanian, V. N. 2018. Grad-cam++: Generalized gradient-based visual explanations for deep convolutional networks. In *2018 IEEE winter conference on applications of computer vision (WACV)*, 839–847. IEEE.

Chefer, H.; Gur, S.; and Wolf, L. 2021. Transformer interpretability beyond attention visualization. In *Proceedings of the IEEE/CVF conference on computer vision and pattern recognition*, 782–791.

Chen, L.; Zhang, Y.; Song, Y.; Liu, L.; and Wang, J. 2022. Self-supervised learning of adversarial example: Towards good generalizations for deepfake detection. In *IEEE Conference on Computer Vision and Pattern Recognition*, 18710–18719.

Chen, S.; Yao, T.; Chen, Y.; Ding, S.; Li, J.; and Ji, R. 2021. Local relation learning for face forgery detection. In *AAAI Conference on Artificial Intelligence*, volume 35, 1081–1088.

Chen, Z.; Sun, K.; Zhou, Z.; Lin, X.; Sun, X.; Cao, L.; and Ji, R. 2024. DiffusionFace: Towards a Comprehensive Dataset for Diffusion-Based Face Forgery Analysis. *arXiv preprint arXiv:2403.18471*.

Cheng, J.; Yan, Z.; Zhang, Y.; Hao, L.; Ai, J.; Zou, Q.; Li, C.; and Wang, Z. 2025a. Stacking brick by brick: Aligned feature isolation for incremental face forgery detection. In *IEEE Conference on Computer Vision and Pattern Recognition*, 13927–13936.

Cheng, J.; Yan, Z.; Zhang, Y.; Luo, Y.; Wang, Z.; and Li, C. 2024. Can we leave deepfake data behind in training deepfake detector? *Advances in Neural Information Processing Systems*, 37: 21979–21998.

Cheng, J.; Zhang, Y.; Zou, Q.; Yan, Z.; Liang, C.; Wang, Z.; and Li, C. 2025b. Ed ^4: Explicit data-level debiasing for deepfake detection. *IEEE Transactions on Image Processing*.

Cui, X.; Li, Y.; Luo, A.; Zhou, J.; and Dong, J. 2025a. Forensics Adapter: Adapting CLIP for Generalizable Face Forgery Detection. In *IEEE/CVF Conference on Computer Vision and Pattern Recognition*, 19207–19217.

Cui, X.; Li, Y.; Luo, A.; Zhou, J.; and Dong, J. 2025b. Forensics adapter: Adapting clip for generalizable face forgery detection. In *IEEE Conference on Computer Vision and Pattern Recognition Conference*, 19207–19217.

Deng, J.; Guo, J.; Xue, N.; and Zafeiriou, S. 2019. Arcface: Additive angular margin loss for deep face recognition. In *Proceedings of the IEEE Conference on Computer Vision and Pattern Recognition*, 4690–4699.

Dolhansky, B.; Bitton, J.; Pflaum, B.; Lu, J.; Howes, R.; Wang, M.; and Ferrer, C. C. 2020. The deepfake detection challenge (dfdc) dataset. *arXiv preprint arXiv:2006.07397*.

Dong, S.; Wang, J.; Ji, R.; Liang, J.; Fan, H.; and Ge, Z. 2023. Implicit identity leakage: The stumbling block to improving deepfake detection generalization. In *Proceedings of the IEEE Conference on Computer Vision and Pattern Recognition*, 3994–4004.

Guo, J.; Zhu, X.; Zhao, C.; Cao, D.; Lei, Z.; and Li, S. Z. 2020. Learning meta face recognition in unseen domains. In *IEEE Conference on Computer Vision and Pattern Recognition*, 6163–6172.

Huang, B.; Wang, Z.; Yang, J.; Ai, J.; Zou, Q.; Wang, Q.; and Ye, D. 2023. Implicit Identity Driven Deepfake Face Swapping Detection. In *IEEE Conference on Computer Vision and Pattern Recognition*, 4490–4499.

Kashiani, H.; Talemi, N. A.; and Afghah, F. 2025. Freqdebias: Towards generalizable deepfake detection via consistency-driven frequency debiasing. In *IEEE Conference on Computer Vision and Pattern Recognition*, 8775–8785. IEEE.

Kim, M.; Tariq, S.; and Woo, S. S. 2021. Cored: Generalizing fake media detection with continual representation using distillation. In *ACM International Conference on Multimedia*, 337–346.

Li, L.; Bao, J.; Zhang, T.; Yang, H.; Chen, D.; Wen, F.; and Guo, B. 2020a. Face x-ray for more general face forgery detection. In *IEEE Conference on Computer Vision and Pattern Recognition*, 5001–5010.

Li, Y.; Chang, M.-C.; and Lyu, S. 2018. In ictu oculi: Exposing ai created fake videos by detecting eye blinking. In *IEEE International Workshop on Information Forensics and Security*, 1–7.

Li, Y.; Yang, X.; Sun, P.; Qi, H.; and Lyu, S. 2020b. Celeb-df: A large-scale challenging dataset for deepfake forensics. In *IEEE Conference on Computer Vision and Pattern Recognition*, 3207–3216.

Li, Z.; and Hoiem, D. 2017. Learning without forgetting. *IEEE Transactions on Pattern Analysis and Machine Intelligence*, 40(12): 2935–2947.

Liang, J.; Shi, H.; and Deng, W. 2022. Exploring disentangled content information for face forgery detection. In *European Conference on Computer Vision*, 128–145. Springer.

Luo, Z.; Liu, Y.; Schiele, B.; and Sun, Q. 2023. Class-incremental exemplar compression for class-incremental learning. In *IEEE Conference on Computer Vision and Pattern Recognition*, 11371–11380.

McInnes, L.; Healy, J.; and Melville, J. 2018. Umap: Uniform manifold approximation and projection for dimension reduction. *arXiv preprint arXiv:1802.03426*.

Nick Dufour, G. R.; and Andrew Gully, J. 2019. Deep Fake Detection Dataset. https://ai.googleblog.com/2019/09/contributing-data-to-deepfake-detection.html.

Pan, K.; Yin, Y.; Wei, Y.; Lin, F.; Ba, Z.; Liu, Z.; Wang, Z.; Cavallaro, L.; and Ren, K. 2023. Dfil: Deepfake incremental learning by exploiting domain-invariant forgery clues. In *ACM International Conference on Multimedia*, 8035–8046.

Qian, Y.; Yin, G.; Sheng, L.; Chen, Z.; and Shao, J. 2020. Thinking in frequency: Face forgery detection by mining frequency-aware clues. In *European Conference on Computer Vision*, 86–103. Springer.

Radford, A.; Kim, J. W.; Hallacy, C.; Ramesh, A.; Goh, G.; Agarwal, S.; Sastry, G.; Askell, A.; Mishkin, P.; Clark, J.; et al. 2021. Learning transferable visual models from natural language supervision. In *International conference on machine learning*, 8748–8763. PMLR.

Rebuffi, S.-A.; Kolesnikov, A.; Sperl, G.; and Lampert, C. H. 2017. icarl: Incremental classifier and representation learning. In *IEEE Conference on Computer Vision and Pattern Recognition*, 2001–2010.

Rossler, A.; Cozzolino, D.; Verdoliva, L.; Riess, C.; Thies, J.; and Nießner, M. 2019. Faceforensics++: Learning to detect manipulated facial images. In *IEEE International Conference on Computer Vision*, 1–11.

Selvaraju, R. R.; Cogswell, M.; Das, A.; Vedantam, R.; Parikh, D.; and Batra, D. 2017. Grad-cam: Visual explanations from deep networks via gradient-based localization. In *Proceedings of the IEEE international conference on computer vision*, 618–626.

Shiohara, K.; and Yamasaki, T. 2022. Detecting deepfakes with self-blended images. In *IEEE Conference on Computer Vision and Pattern Recognition*, 18720–18729.

Sun, K.; Chen, S.; Yao, T.; Sun, X.; Ding, S.; and Ji, R. 2025. Continual face forgery detection via historical distribution preserving. *International Journal of Computer Vision*, 133(3): 1067–1084.

Sun, K.; Yao, T.; Chen, S.; Ding, S.; Li, J.; and Ji, R. 2022. Dual contrastive learning for general face forgery detection. In *AAAI Conference on Artificial Intelligence*, volume 36, 2316–2324.

Tian, J.; Yu, C.; Wang, X.; Chen, P.; Xiao, Z.; Han, J.; and Chai, Y. 2024. Dynamic mixed-prototype model for incremental deepfake detection. In *ACM International Conference on Multimedia*, 8129–8138.

Wang, C.; and Deng, W. 2021. Representative forgery mining for fake face detection. In *IEEE Conference on Computer Vision and Pattern Recognition*, 14923–14932.

Wang, H.; Wang, Y.; Zhou, Z.; Ji, X.; Gong, D.; Zhou, J.; Li, Z.; and Liu, W. 2018. CosFace: Large Margin Cosine Loss for Deep Face Recognition. In *IEEE Conference on Computer Vision and Pattern Recognition*, 5265–5274.

Wang, L.; Zhang, X.; Yang, K.; Yu, L.; Li, C.; Hong, L.; Zhang, S.; Li, Z.; Zhong, Y.; and Zhu, J. 2022. Memory replay with data compression for continual learning. *arXiv preprint arXiv:2202.06592*.

Yan, S.; Xie, J.; and He, X. 2021. Der: Dynamically expandable representation for class incremental learning. In *IEEE Conference on Computer Vision and Pattern Recognition*, 3014–3023.

Yan, Z.; Luo, Y.; Lyu, S.; Liu, Q.; and Wu, B. 2024a. Transcending forgery specificity with latent space augmentation for generalizable deepfake detection. In *IEEE Conference on Computer Vision and Pattern Recognition*, 8984–8994.

Yan, Z.; Wang, J.; Jin, P.; Zhang, K.-Y.; Liu, C.; Chen, S.; Yao, T.; Ding, S.; Wu, B.; and Yuan, L. 2025a. Orthogonal Subspace Decomposition for Generalizable AI-Generated Image Detection. In *International Conference on Machine Learning*, 70268–70288.

Yan, Z.; Wang, J.; Wang, Z.; Jin, P.; Zhang, K.-Y.; Chen, S.; Yao, T.; Ding, S.; Wu, B.; and Yuan, L. 2025b. Effort: Efficient orthogonal modeling for generalizable ai-generated image detection. In *International Conference on Machine Learning*.

Yan, Z.; Yao, T.; Chen, S.; Zhao, Y.; Fu, X.; Zhu, J.; Luo, D.; Yuan, L.; Wang, C.; Ding, S.; et al. 2024b. DF40: Toward Next-Generation Deepfake Detection. *arXiv preprint arXiv:2406.13495*.

Yan, Z.; Zhang, Y.; Fan, Y.; and Wu, B. 2023a. UCF: Uncovering Common Features for Generalizable Deepfake Detection. In *IEEE International Conference on Computer Vision*, 22412–22423.

Yan, Z.; Zhang, Y.; Yuan, X.; Lyu, S.; and Wu, B. 2023b. Deepfakebench: A comprehensive benchmark of deepfake detection. *arXiv preprint arXiv:2307.01426*.

Zhang, X.; Zhu, P.; Zhang, C.; Yan, Z.; Cheng, J.; Lao, M.; Cai, S.; and Guo, Y. 2025. Generalization-Preserved Learning: Closing the Backdoor to Catastrophic Forgetting in Continual Deepfake Detection. In *Proceedings of the IEEE/CVF International Conference on Computer Vision*, 3798–3808.

Zhao, H.; Zhou, W.; Chen, D.; Wei, T.; Zhang, W.; and Yu, N. 2021. Multi-attentional deepfake detection. In *IEEE Conference on Computer Vision and Pattern Recognition*, 2185–2194.

Zhou, Y.; He, X.; Lin, K.; Fan, B.; Ding, F.; and Li, B. 2026. Simplicity Prevails: The Emergence of Generalizable AIGI Detection in Visual Foundation Models. *arXiv preprint arXiv:2602.01738*.

Zi, B.; Chang, M.; Chen, J.; Ma, X.; and Jiang, Y.-G. 2020. Wilddeepfake: A challenging real-world dataset for deepfake detection. In *ACM International Conference on Multimedia*, 2382–2390.

Appendix

1 Related Work

1.1 Face Forgery Detection

Existing generalization-oriented face forgery detection methods typically leverage a limited set of known forged samples to train a generic detector capable of handling unseen forgery types. Early studies primarily enhance discriminative capability by exploiting explicit forgery-related patterns, such as noise artifacts (Li et al. 2020a), local region cues (Chen et al. 2021; Zhao et al. 2021), and frequency-domain information (Qian et al. 2020; Guo et al. 2020; Kashiani, Talemi, and Afghah 2025). As forgery techniques become increasingly realistic, explicit artifacts tend to diminish, shifting research focus toward mining implicit forgery patterns. To this end, a variety of learning strategies have been proposed, including contrastive learning (Sun et al. 2022), identity-aware modeling (Huang et al. 2023; Dong et al. 2023), disentangled representation learning (Liang, Shi, and Deng 2022; Yan et al. 2023a), reconstruction-based learning (Cao et al. 2022; Wang and Deng 2021), and diverse data augmentation techniques (Chen et al. 2022; Shiohara and Yamasaki 2022; Yan et al. 2024a). More recently, several approaches based on vision Transformers have leveraged vision–language models, such as CLIP (Cui et al. 2025b) and the LoRA-based Effort (Yan et al. 2025b), to further enhance generalization performance. Overall, existing approaches strive to derive forgery-aware representations that generalize beyond known manipulations. Yet, due to the limited coverage of current forgery datasets, detectors trained under a static offline setting struggle to remain effective when confronted with continuously emerging forgery techniques.

1.2 Incremental Learning for Forgery Detection

Incremental learning has been widely applied to mitigate catastrophic forgetting, with replay-based strategies dominating the incremental face forgery detection. These methods store or reuse representative samples from previous tasks and employ various enhancements to preserve prior knowledge. For instance, CoReD (Kim, Tariq, and Woo 2021) uses knowledge distillation to retain information from past tasks. DFIL (Pan et al. 2023) prioritizes central and challenging samples to maximize the value of replayed data. HDP (Sun et al. 2025) leverages carefully crafted universal adversarial perturbations for more robust replay. DMP (Tian et al. 2024) summarizes previous distributions through mixed prototypes. The most recent method, SUR-LID (Cheng et al. 2025a), combines sparse uniform replay with a latent-space incremental detector to further consolidate prior knowledge. While effective, all of these approaches rely on explicit access to stored historical data, which imposes non-negligible memory overhead and raises potential privacy concerns.

In continual learning, several studies have explored compressed replay to reduce storage cost and store more historical samples under a fixed memory budget, such as compressing exemplars by removing non-discriminative pixels (Luo et al. 2023) or selecting an appropriate compression quality for replay (Wang et al. 2022). However, existing compressed replay methods are largely developed for generic class-incremental settings and typically operate at the image or pixel level, without explicitly considering the task-specific structure of face forgery detection. In this domain, replay is expected to preserve identity cues, forgery traces, and domain-specific patterns that may exhibit distinct spatial distributions, suggesting that more tailored replay compression strategies still remain to be explored.

2 Discussion on Real-World Actual Storage Consumption

Considering that the core objective of this work is to minimize storage consumption in real-world scenarios as much as possible, it is necessary to rigorously analyze the relationship between storage cost and the replay representation from a practical perspective.

Intuitively, one may assume that reducing the effective pixels of a single image by $n\%$ would naturally lead to an equivalent $n\%$ reduction in storage. However, this assumption does not hold in practice. A single sector-shaped region cannot be directly stored as a standalone PNG file. Moreover, simply setting invalid pixels to zero or one does not yield a real reduction in storage cost due to the underlying image encoding mechanism.

To bridge the gap between pixel reduction and actual storage reduction, we adopt a simple yet effective storage strategy. Specifically, instead of storing the masked image directly, we represent each row of the cropped region as a variable-length array containing only the valid pixel values. Combined with the original image resolution, the learnable segment can then be reconstructed online during training, while ensuring that the storage reduction strictly matches the targeted $n\%$. This design is enabled by the structural property of the ClockMix cropping region, which is always contiguous along *one side* of the image boundary. In other words, for every row, the starting horizontal coordinate must be either 0 or $(1 - \text{len})$, where (len) denotes the valid length of that row. Therefore, we only need to store an additional binary flag per image to indicate whether the segment starts from 0 or from $(1 - \text{len})$. This 1-bit overhead is negligible in practice, yet it allows for lossless reconstruction of the original segment.

In summary, the proposed percentage reduction of the replay region can be translated into a proportional reduction in actual storage cost in practical deployment settings.

3 Algorithm

Here, we provide the replay storing details of the proposed InfoDense via Alg. 1, which includes cutting and selection.

4 Detailed Implementation Settings

4.1 Preprocessing

Data Preprocessing. Following the standard DeepFakeBench (Yan et al. 2023b) protocol, all video frames from all datasets undergo face detection, extraction, and alignment before being resized to 224×224. For input normalization, we adopt a mean of $[0.4815, 0.4578, 0.4082]$ and a standard deviation of $[0.2686, 0.2613, 0.2758]$ for the three RGB channels, which are adopted by the official CLIP-series

Algorithm 1: Replay Storing Algorithm of InfoDense

Require: Previous-task dataset $\mathbb{I}^{t-1}$; trained detector $f(\cdot, \theta^{t-1})$; forgery text embedding $\mathbf{z}_f$; replay size m; weight λ.
Ensure: Final replay set $\mathbf{S}^{t-1}$.

Initialize the candidate set $\mathbf{S} \leftarrow \emptyset$.
for $\mathbf{x}_i \in \mathbb{I}^{t-1}$ **do**
  Extract image tokens:

$$\{\mathbf{z}_{cls}, \mathbf{z}_{(1,1)}, \ldots, \mathbf{z}_{(n,n)}\} = E(\mathbf{x}_i).$$

  Compute the forgery-decisive score of each patch:

$$\delta_{(u,v)} = \mathrm{Sim}(\mathbf{z}_{(u,v)}, \mathbf{z}_f).$$

  Select the top-10 decisive patches:

$$\mathbf{P}_D^i \leftarrow \mathrm{Top}_{10}\big(\{\mathbf{p}_{(u,v)}\}, \delta_{(u,v)}\big).$$

  Find the segment containing the maximum number of decisive patches:

$$\alpha_i^* = \underset{\alpha \in [0,\, 360-360/n)}{\arg\max} \mathrm{Count}_D\big(\mathrm{Seg}(v_1, v_2, \alpha)\big).$$

  Extract the corresponding segment:

$$\mathbf{s}_i = \mathrm{Seg}(\mathbf{x}_i, v_1, v_2, \alpha_i^*).$$

  $\mathbf{S} \leftarrow \mathbf{S} \cup \{(\mathbf{s}_i, \mathbf{x}_i)\}$.
end for
Compute the feature centroid:

$$\mathbf{c} = \frac{1}{|\mathbb{I}^{t-1}|} \sum_{\mathbf{x}_i \in \mathbb{I}^{t-1}} f(\mathbf{x}_i).$$

for $(\mathbf{s}_i, \mathbf{x}_i) \in \mathbf{S}$ **do**
  Compute representativeness and decisive-patch density:

$$R_i = \cos(\mathbf{c}, f(\mathbf{x}_i)), \qquad D_i = \mathrm{Count}_D(\mathbf{s}_i).$$

end for
Normalize $\{R_i\}$ and $\{D_i\}$ to $[0, 1]$, obtaining $\widetilde{R}_i$ and $\widetilde{D}_i$.
Compute the selection score:

$$\mathrm{Score}(\mathbf{s}_i) = \lambda \widetilde{R}_i + (1 - \lambda)\widetilde{D}_i.$$

Select the top-m segments:

$$\mathbf{S}^{t-1} = \mathrm{Top}_m\big(\mathbf{S}, \mathrm{Score}(\mathbf{s}_i)\big).$$

models (Radford et al. 2021). During training, 8 frames are uniformly sampled from each video, while 32 frames are sampled during testing to ensure more stable and reliable performance evaluation, as well as alignment with baselines.

Data Augmentation. To enhance the generalization ability of the detector, we employ a comprehensive data augmentation pipeline on the current task data using the `Albumentations (Buslaev et al. 2020)` library. The augmentation operations and their corresponding application probabilities are detailed as follows:

- **Spatial Transformations:** Horizontal Flip ($p = 0.5$), Rotation within $\pm 10^\circ$ ($p = 0.5$), and isotropic resizing.
- **Pixel-level Transformations:** Gaussian Blur with a kernel size in the range of $[3, 7]$ ($p = 0.5$).
- **Compression Artifacts:** JPEG compression with a quality range of 40–100, applied with $p = 0.5$.
- **Color Perturbations:** One of Random Brightness/Contrast (limit 0.1), FancyPCA, or HueSaturationValue, selected and applied with probability $p = 0.5$.

It is worth noting that while the current task data are augmented as described above, the generated replay samples are kept with standard normalization only so as to preserve their intrinsic generative distribution characteristics.

4.2 Batch Composition and Fusion Details

To ensure strict class balance during the incremental learning process, we employ a paired sampling strategy for the current-task data. Within each training step, the base batch is explicitly enforced to contain an equal quantity of intact pristine and manipulated images, denoted as B_r real samples and B_f fake samples. To promote model desensitization to artificial fusion boundaries, we first construct intra-task mixed samples. Given a spatial compression rate γ, which represents the reciprocal of the retained sector angle, we synthesize $\lfloor B_r/\gamma \rfloor$ intra-task real-fused samples alongside $\lfloor B_f/\gamma \rfloor$ intra-task fake-fused samples directly from the current batch. Furthermore, to consolidate historical knowledge,

we execute inter-task fusion governed by a replay batch parameter B_{rep}. Specifically, we sample localized fragments from the memory buffer and fuse them onto current-task images, yielding three distinct cross-task combinations to prevent class bias: B_{rep} samples combining previous real with current real, B_{rep} samples combining previous fake with current fake, and B_{rep} samples combining previous fake with current real. All aforementioned fused variants, together with the original intact samples, constitute the final comprehensive mini-batch for detector optimization.In our implementation, we empirically set $B_r = 8$ and $B_{rep} = 4$.

5 Further Analysis and Ablations

5.1 Performance Evaluation under Aligned Buffer Sizes

To provide a complementary perspective to the storage-aligned Pareto analysis in Fig. 4, we further evaluate the performance by strictly aligning the replay buffer size (*i.e.*, the absolute numerical quantity of stored samples). As shown in Fig. 7, when utilizing moderate compression rates ($n \in \{2, 3, 4\}$), the InfoDense strategy consistently matches or surpasses the full-image baseline across varying buffer capacities. This phenomenon reveals that full images inherently contain task-irrelevant background noise and dataset-specific biases that can hinder incremental learning. By proactively filtering out these redundancies, moderate density-aware extraction provides a purer, more concentrated supervision signal. Conversely, excessively aggressive compression ($n = 5$ or 10) causes performance to drop below the baseline, indicating that extreme spatial reduction inevitably discards essential forgery artifacts alongside the background. Therefore, appropriate regional extraction acts as a powerful regularization mechanism that mitigates domain-specific redundancy while retaining core discriminative clues, thereby yielding strong generalization even without the advantage of an expanded sample capacity.

5.2 Sensitivity Analysis of Decisive Patches

We conduct a sensitivity analysis on the number of decisive patches K used during density-aware extraction. As shown in Fig. 8, the incremental detection performance reaches its best result at $K = 10$ and degrades when K is either too small or too large. This trend supports our facial redundancy hypothesis that a limited number of decisive patches is sufficient to preserve the forgery-related information required for incremental learning. Specifically, when K is too small (*e.g.*, $K = 5$), the selected region may fail to cover some fine-grained forgery artifacts. In contrast, a larger K (*e.g.*, $K = 20$) introduces more identity-related and task-irrelevant facial regions, reducing the information density of the extracted segment. Overall, $K = 10$ provides the best trade-off between preserving discriminative forgery cues and avoiding unnecessary spatial redundancy.

6 Qualitative Visualization

To intuitively demonstrate the density-aware extraction process, Figure 10 provides a step-by-step visualization of how InfoDense progressively compresses each input face. Our method accurately localizes fine-grained forgery artifacts and removes task-irrelevant background regions, thereby achieving substantial storage compression while preserving the essential discriminative clues required for effective replay.

Table 5: Frozen CLIP for intrinsic forgery capability.

Method	FF++	CDFv2	Avg.
CLIP+Linear	87.33	94.54	90.94

7 Additional Experimental Results

7.1 Robustness against Image Degradations

To verify that the proposed regional decisive replay mechanism does not overfit to high-quality pristine data, we evaluate its robustness against common real-world image degradations. During the inference phase, we independently apply four types of perturbations, including downsampling, saturation alteration, block-wise drop, and JPEG compression. Each degradation is designed with five progressive severity levels to comprehensively assess the performance decay trend, with average AUC as the evaluation metric. As shown in Fig. 9, InfoDense consistently exhibits superior resilience against varying degrees of corruption compared to the baseline. This demonstrates that by selectively replaying information-dense regions, the model reduces reliance on fragile artifacts and successfully learns robust forgery traces.

7.2 Prompt and CLIP Intrinsic Knowledge for Forgery Awareness

The decisive-patch score is computed using a forgery-trained CLIP, rather than an untouched zero-shot CLIP. Namely, the score is not used in the first task, but only in subsequent tasks where *replay* is required, by which time the model has *already* learned forgery-awareness from previous tasks.

Moreover, the pretrained CLIP representation already contains forgery-discriminative information. Prior works (Cui et al. 2025a; Zhou et al. 2026; Yan et al. 2025a) and our Table 5 support that a frozen pretrained CLIP backbone with only a trained LoRA and linear classifier can achieve strong detection, suggesting its intrinsic non-trivial forgery separability. Therefore, we adopt a frozen backbone with an Adapter that can preserve the overall representation structure and text-image alignment ability of CLIP, with "this image is [Learn-Token] {real, fake}" as the prompts.

The score is guiding as a *better-than-random* prior for selecting more informative regions, not as a precise forgery mask estimator. Hence, it is sufficient for the score to prioritize artifact-rich regions; occasional sub-optimal selections do not fundamentally undermine our method. Meanwhile, Fig. 10 shows the effectiveness of leveraging CLIP-similarity to localize forgery regions.

7.3 Weight Ablation and Fragment Number Analysis

In practice, we normalize both terms to $[0, 1]$ before combination. Table 6 reports the results with different values of

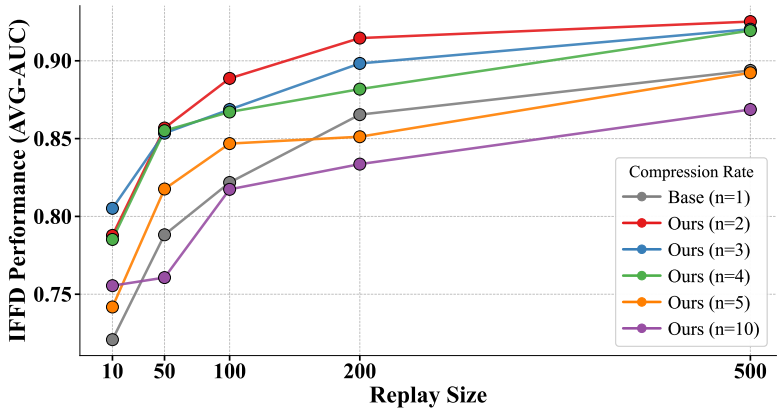

Figure 7: Performance comparison strictly aligned by the replay buffer size.

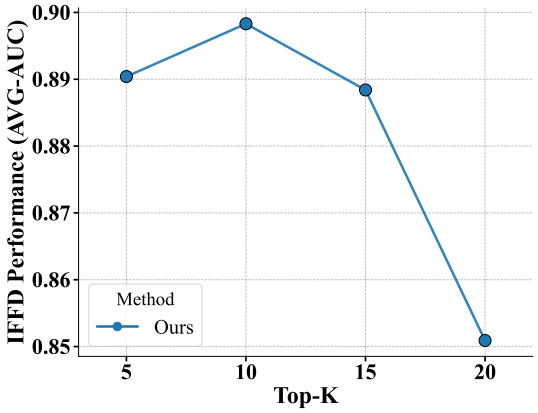

Figure 8: Sensitivity analysis on the number of decisive patches K.

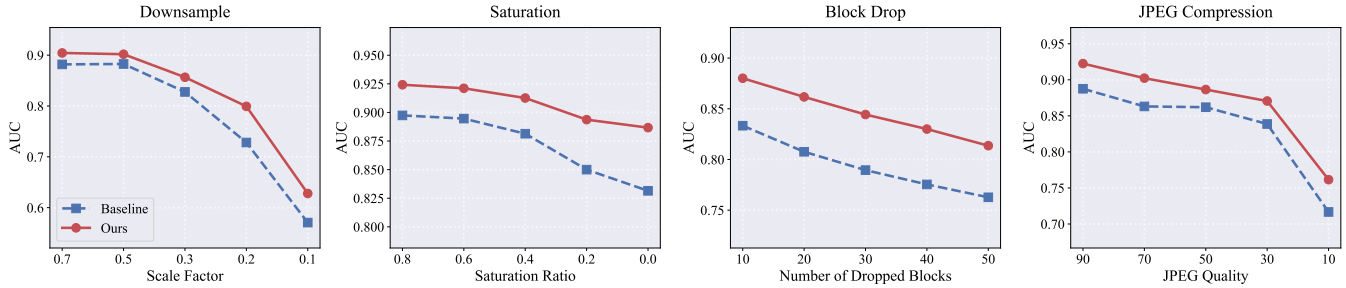

Figure 9: Robustness evaluation against test-time common image degradations across five progressive severity levels.

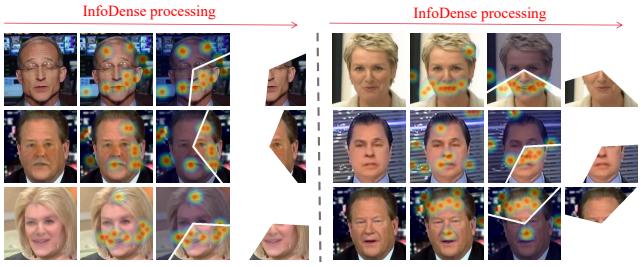

Figure 10: Visualization of InfoDense extraction. From left to right: (a) Original face. (b) Top-K decisive patches. (c) Cropping region. (d) Final InfoDense replay segment.

λ in Eq. (4). The results show that jointly considering representativeness and decisive-patch density is more effective than relying on either term alone, with $\lambda = 0.5$ used as our default setting.

We also analyze whether selecting multiple fragments from one image is beneficial. As shown in the lower half of Table 6, selecting two or three fragments from the same image degrades performance, possibly because excessive fragmentation disrupts local forgery structures.

7.4 Analysis of the Fan-shaped Region Strategy

Since artifact characters in one sample are usually similar, InfoDense does not aim to preserve all forgery regions within a sample. Instead, it retains the most information-dense intact region while discarding less informative regions to improve replay efficiency. The fan-shape covers face and context simultaneously, including facial landmarks, boundaries, blending clues, and background. Table 7 shows that it outperforms alternative region-selection strategies.

7.5 Quantitative Definition of Information Density

Theoretically, InfoDense can be regarded as semantic-guided replay distillation, aiming to maximize discriminative information per storage unit rather than preserve raw pixels. We define *information density* as

$$D(s) = \frac{1}{|s|} \sum_{p \in P_D} \mathbb{I}(p \in s), \tag{6}$$

where P_D denotes forgery-decisive patches. The regional selection ablation quantitatively shows that InfoDense outperforms random, center-based, and center+hard segment selection, demonstrating the effectiveness of jointly considering representativeness and forgery-information density.

7.6 Comparison under Prior Incremental Protocols

We further report the protocol aligned with prior works, including DevFD, with lower-triangular stage-wise metrics. This protocol uses the sequence FF++, DFDCP, DFD, and

Table 6: Upper half: ablation on λ in Eq. (4), where λ weights representativeness and $1-\lambda$ weights decisive-patch density. Lower half: "Frag=2" denotes selecting two different fragments from each image.

Setting	Incremental Dataset					Cross-dataset				
	FF++	DFDCP	CDF	AA ↑	AF ↓	SDv21	UADFV	WDF	DFD	Avg.
$\lambda = 0$	82.29	88.51	96.97	89.25	7.85	93.06	92.46	72.76	82.49	85.19
$\lambda = 1/3$	83.01	87.65	97.59	89.41	7.67	82.01	**96.60**	75.33	86.27	85.05
$\lambda = 2/3$	78.10	82.89	94.56	85.18	11.67	76.25	83.68	71.09	78.98	77.50
Frag=2	82.25	**89.81**	95.97	89.34	7.43	92.60	95.05	71.01	84.55	85.80
Frag=3	80.71	85.19	96.96	87.62	8.86	91.19	91.65	73.10	78.99	83.73
Ours ($\lambda = 0.5$)	**84.11**	89.41	**97.75**	**90.42**	**6.03**	**97.88**	94.71	**79.38**	**88.13**	**90.03**

Table 7: Comparison of different region construction strategies. LM denotes facial landmark guidance.

Method	Cross-dataset AUC (%)		
	DFD	CDF-v2	Avg.
Mosaic	71.01	59.39	65.20
CutMix	83.99	78.62	81.31
Mixup	81.67	75.75	78.71
LM-Guided	84.09	80.81	82.45
Fan-shaped (Ours)	**87.65**	**83.94**	**85.80**

CDF2. The results show that our method remains competitive under prior protocols while still achieving strong final-stage average performance overall.

Table 8: Protocol aligned with prior works, including DevFD, with lower-triangular stage-wise matrix.

Method	Dataset	Acc(%) ↑				Avg. ↑	AF ↓
		FF++	DFDCP	DFD	CDF2		
DMP	FF++	95.96	-	-	-	95.96	-
	DFDCP	92.71	89.72	-	-	91.22	3.25
	DFD	**92.64**	86.09	94.84	-	91.19	3.48
	CDF2	**91.61**	84.86	91.81	91.67	89.99	4.08
DevFD	FF++	**98.41**	-	-	-	**98.41**	-
	DFDCP	**97.06**	89.90	-	-	**93.48**	**1.35**
	DFD	92.44	**89.07**	**97.91**	-	**93.14**	**3.40**
	CDF2	90.71	**90.31**	93.12	85.15	89.82	4.03
Ours	FF++	95.02	-	-	-	95.02	-
	DFDCP	92.12	**90.49**	-	-	91.31	2.90
	DFD	88.99	88.49	97.82	-	91.77	4.02
	CDF2	87.73	89.96	**95.27**	**96.05**	**92.61**	**3.46**

7.7 Additional AA/AF Metrics

We further provide AA/AF results and lower-triangular stage-wise metrics. As shown in Figure 11 and Table 8, our method achieves stability under incremental learning.

7.8 Computation Overhead

InfoDense is efficient and GPU-free, adding only **0.32h** training overhead, corresponding to **2.70%**. Our FLOPs remain unchanged since the base model is unmodified.

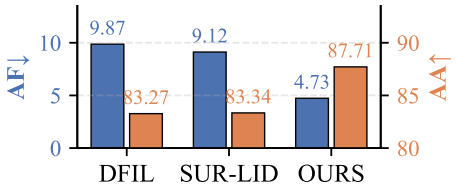

Figure 11: AA/AF results.

7.9 Privacy Analysis of Fused Training Samples

Although InfoDense stores only fragmented facial regions, InfoFuse reconstructs complete training samples by combining historical fragments with current-task images. We therefore further examine whether these fused samples reveal the identities of their source faces. Specifically, we use ArcFace and CosFace to retrieve the corresponding original identities and report Top-1/Top-3 retrieval recall and identity similarity (IDSim). Lower values indicate less identity information leakage. As shown in Table 9, all retrieval recalls remain below 0.02%, while the identity similarities are close to zero under both recognition models. These results demonstrate that the fused training samples do not preserve identifiable facial representations and thus provide strong protection against identity leakage.

Table 9: Identity leakage analysis of fused training samples. Lower values indicate better privacy preservation.

Metric ↓	ArcFace	CosFace
Recall@1 (%)	0.01	0.01
Recall@3 (%)	0.02	0.01
IDSim	0.0071	0.0095